International Journal of Mass Spectrometry 277 (2008) 197–205

Contents lists available at ScienceDirect

International Journal of Mass Spectrometry

journal homepage: www.elsevier.com/locate/ijms

Collision induced fragmentation of free sulfur clusters

Tiberiu Arion[a], Roman Flesch[a], Thomas Schlathölter[b], Fresia Alvarado[b], Ronnie Hoekstra[b], Reinhard Morgenstern[b], Eckart Rühl[a,*]

[a] Physikalische Chemie, Institut für Chemie und Biochemie, Freie Universität Berlin, Takustr. 3, 14195 Berlin, Germany
[b] KVI Atomic Physics, University of Groningen, Zernikelaan 25, 9747 AA Groningen, The Netherlands

ARTICLE INFO

Article history:
Received 7 March 2008
Received in revised form 7 June 2008
Accepted 13 June 2008
Available online 21 June 2008

Keywords:
Fragmentation
Highly charged ion
Fission
Sulfur cluster

ABSTRACT

Fragmentation of multiply charged sulfur clusters is investigated by ion–ion-coincidence spectroscopy. The experiments were performed at the electron cyclotron resonance (ECR) ion source at the KVI Groningen, where beams of Xe^{q+} (q = 5, 10, 15, 20) were produced. The Xe^{q+} ions were accelerated to kinetic energies of 8–10·q keV and collided with a beam of free sulfur clusters. Variable size sulfur clusters are prepared in a two-stage oven source, where the temperature of the oven was used to adjust the cluster size. Most experiments were performed using S_8, the dominant cluster at low oven temperature. Ion–ion-coincidence as well as mass spectra were recorded. Coincidences between singly charged atomic and molecular fragments were studied, where changes of product channels were observed as a function of charge state of the Xe^{q+} projectile. The mechanisms of cluster fragmentation are discussed. The results are compared to earlier experiments on core-excited sulfur clusters using soft X-rays.

1. Introduction

Clusters are known to bridge the gap between isolated atoms or molecules and condensed matter. Structural and electronic properties of clusters have been investigated in the past, revealing size- and material-dependent properties [1–3]. This also includes fragmentation of clusters, where size-dependent fragmentation mechanisms have been explored before [4–6]. Fragmentation of clusters is often induced by ionizing radiation, high kinetic energy electrons, laser radiation, or highly charged ions (HCI) [7–10]. The mechanisms leading to the formation of stable products are sensitive to the primary excitation process [6]. This is particularly true for the formation and decay of doubly or multiply charged clusters, for which fission and Coulomb explosion scenarios have been discussed [11,12]. Depending on the cluster material, charge equilibration or charge localization is observed upon multiple ionization, the latter being important in the context of multiple ionization of van der Waals clusters [6]. However, experimental studies employing neutral van der Waals clusters have the inherent disadvantage that the cluster size distribution is broad, so that size-dependent fission pathways cannot be easily inferred from experimental work. In contrast, covalently bound clusters can often be prepared in well-defined sizes via the evaporation from the solid phase [13–18]. As a result, covalently bound clusters are suitable model systems to experimentally investigate fragmentation and fission properties of ionized clusters. Chalcogenide clusters have been previously investigated in the S 2p and the S 1s-excitation regimes [13–18]. Fission mechanisms of doubly and multiply charged sulfur clusters, occurring after core hole relaxation and the emission of Auger electrons, have been derived for S 2p-excited sulfur clusters using photoelectron-photoion–photoion coincidence (PEPIPICO) spectroscopy [16]. This approach provides sets of coincidence data, which allow one to derive the fission mechanisms.

Here, we apply the same technique to investigate S_n ionization by highly charged ions which also leads to the removal of outer valence electrons. The ionization process is thus similar to inner-shell excitation by photons which is followed by the emission of Auger electrons. Subsequently, the formed multiply charged ions are stabilized via fission.

Different fission pathways may occur in ionization induced by HCI or by inner-shell photoexcitation, respectively, depending on the primary vacancy formation process and the nature of the vacancies. Evidence for such differences comes from earlier multiple coincidence work on van der Waals clusters, where HCI impact and photoexcitation trigger fundamentally different fragmentation dynamics [6]. Over the recent years, such differences have also been explored for core level excitation and HCI induced ionization of molecular targets [19,20]. In contrast, there are considerably fewer results on covalent clusters [10]. This is the motivation for the present work, where we report mass spectra of sulfur cluster fragments formed upon impact with keV

* Corresponding author. Tel.: +49 30 83852396; fax: +49 30 83852717.
E-mail address: ruehl@chemie.fu-berlin.de (E. Rühl).

1387-3806/$ – see front matter © 2008 Elsevier B.V. All rights reserved.
doi:10.1016/j.ijms.2008.06.007

highly charged ions. The decay of doubly charged sulfur clusters is studied by means of a coincidence technique.

2. Experimental

The experiments were performed at the ZERNIKELEIF facility at the Kernfysisch Versneller Instituut (KVI) in Groningen (The Netherlands) [21]. We have used highly charged ions from the electron cyclotron resonance ion source. The experiments were performed using beams of Xe^{q+} ions with $q = 5$, 10, 15, and 20, which were accelerated by 10 kV and 8 kV, respectively.

Sulfur clusters are obtained from heating neat yellow α-sulfur (Sigma–Aldrich, purity 99.5%) in a two-stage oven, with two independent heating systems located at the body of the oven and at its orifice, respectively. The use of a two-stage oven has the advantage that it allows one to control the cluster size. This is primarily accomplished by controlling the temperature of the second stage near the orifice. The sample flux is adjusted by tuning the temperature of the first heating stage. Systematic investigations of sulfur as a function of the heating temperature have been carried out previously and a strong dependence of the aggregate size on the temperature has been observed [16–18]. In this study we only focus on the low temperature regime ($T \approx 400$ K), which is known to produce mostly S_8 [22–25]. The other neutrals which are known to occur in the gas phase with a sizeable mixing ratio are S_6 and S_7. These are formed at 400 K relative to the dominant S_8 with ~33% and ~15%, respectively [22]. Consistently, the largest cation observed during the experiments is S_8^+, since S_8 is known to produce a stable parent cation upon ionization [16,25]. During the measurements, the temperature of the second heating stage of the oven is kept constant at $T = 405 \pm 3$ K, whereas the first heating stage is kept about 30 K below this temperature. This yields a pressure in the interaction chamber of $2.9 \pm 0.2 \times 10^{-6}$ mbar, with a base pressure of 9.7×10^{-7} mbar.

The cations are extracted by a constant electric field in a Wiley–McLaren type time-of-flight mass spectrometer [26]. The experiments are performed in a chopped beam mode, where the HCI beam is deflected by a pulsed voltage applied to deflector plates right in front of the interaction region with the cluster beam. The corresponding chopper signal is used as a start for cation time-of-flight measurements. This mode allows us to measure time-of-fight mass spectra as well as ion–ion-coincidence spectra. The extraction conditions in the ionization region of the spectrometer are set to a field strength of 310 V/cm in order to obtain a sufficient time spread of the ion flight time in coincidence spectra. This enables us to determine the kinetic energy release (KER) of fission processes. The drawback of using low extraction field strengths is angular discrimination, implying that mostly the cations flying parallel to the axis of the spectrometer are detected, whereas those high kinetic energy ions of low mass flying perpendicular to this axis are less efficiently probed by the multi-channel plate detector.

3. Results and discussion

3.1. Mass spectrometry

Fig. 1 displays a series of time-of-flight mass spectra of a sulfur sample containing mostly S_8, as obtained from the collisions of sulfur vapor with various Xe^{q+} ion beam charges, with $q = 2$, 5, 10, 15, 20 (cf. Table 1). The Xe^{q+} ions are accelerated by 10 kV, except for Xe^{15+}, for which the acceleration potential is set to 8 kV.

One observes for projectiles of low charge state (Xe^{2+}) that the mass spectrum is dominated by light, singly charged sulfur and sulfur cluster ions, such as S_3^+, S_2^+, and S^+. Considering the composition of neutral sulfur vapor which is dominated by S_8 [22,23], it is straightforward to assume that all other ions besides S_8^+ are fragments resulting from the dissociation of S_8. Note that the relative fragment yields are very different from the ones obtained in previous photoexcitation work. In the case of He (I) radiation, S_8^+ is the dominant cation [16], whereas in the S 2p-excitation regime ($E \approx 170$ eV) the S_8^+ peak is weak. The latter observation is similar to the results displayed in Fig. 1. There are, however, distinct differences between photoexcitation and HCI impact induced ionization and fragmentation.

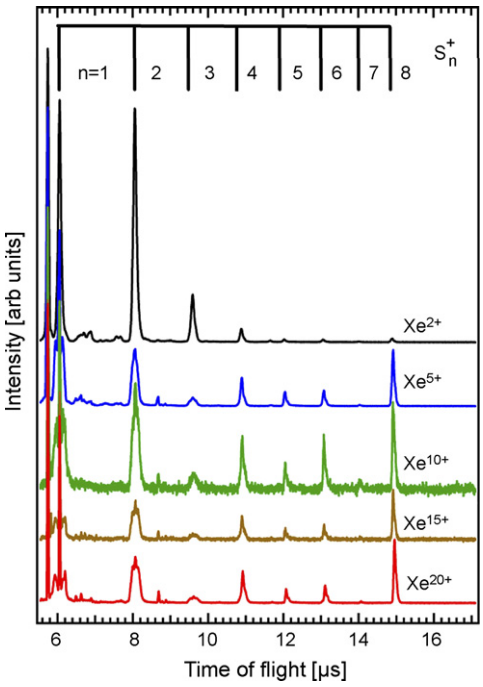

Fig. 1. Time-of-flight mass spectra of S_8 recorded after ionization with various Xe^{q+} ion beams (see results shown in Table 1).

The intensity of the molecular fragments decreases with increasing charge state of the projectile. This implies that fission becomes the dominant process leading to the formation of correlated fragment ions of considerable kinetic energy. Evidence for this assumption will be given below in the context of ion–ion-coincidence experiments. In addition, the $m/q = 32$ peak (S^+: time-of-flight ~6 μs, see Fig. 1), exhibits characteristic wings, which are due to particularly energetic ions, resulting from fission processes. The wings are getting more pronounced with increasing projectile charge state q, being almost absent for $q = 5$ and very pronounced for $q = 20$. In contrast, the neighboring particularly sharp mass peak is due to the residual molecular nitrogen parent ion ($m/q = 28$) which is formed without kinetic energy release. Considering the intensity ratios of the $m/q = 28$ and $m/q = 32$ signals and the mixing ratio of residual gas, it occurs that the $m/q = 32$ peak has two origins. The wings are due to S^+ fragments, whereas the central part of the mass signal is mainly due to O_2^+ from the residual gas. A similar change in peak shape with increasing projectile charge q is observed for the S_2^+ signal, where also wings of high kinetic energy ions are observed (Fig. 1), pointing to fission as the origin of this product ion.

In addition, there is evidence for light ions in the mass spectra obtained after HCI impact (not shown in Fig. 1). These are assigned to be mostly due to multiply charged oxygen, which comes from the fragmentation of water molecules from the residual gas [27,28]. This assignment is supported by intense mass signals of water and its fragments. It cannot be fully excluded that there are also minor

contributions from highly charged sulfur ions since the S/O-mass ratio is ~2. However, also in the coincidence mass spectra there is no visible evidence for correlated fragments involving highly charged sulfur ions. Another point that serves to discard the occurrence of highly charged sulfur ions is the fact that both odd and even sulfur species should occur, similar to earlier work on rare gas clusters [6,9]. There, it was found that a series of multiply charged atomic fragments occurs as a result of cluster fragmentation. This result was explained in terms of charge localization [6], which evidently does not occur in the case of sulfur clusters.

3.2. Chopper-ion–ion coincidence spectroscopy

For investigating the fragmentation of free S_8 after collisions with highly charged ions we have made use of the chopper-ion–ion coincidence technique. The spectrometer was operated such that the flight time t_x of a cation is determined by:

$$t_x = t_0 - \frac{p_z}{F}. \quad (1)$$

The cation flight time t_x depends linearly on its component of the kinetic momentum parallel to the axis of the time-of-flight mass spectrometer p_z. F denotes the extraction force acting on the cation in the ionization region of the spectrometer and t_0 is the flight time of the cation, if it is initially at rest.

The time-of-flight data of two correlated ions recorded in coincidence are loaded into a two-dimensional array of flight times of correlated ions t_1 and t_2, respectively. From these data conclusions regarding the nature of the fragmentation process can be drawn for each correlated ion pair that comes from a doubly charged precursor. Ionization by highly charged ions may also lead to multiply charged sulfur ion clusters, which decay via fission into several charged fragments. These are not discussed in this work, since these processes are found to be weak. The present results show only a weak signal from the correlated cation pair S^{++}/S^+, which requires a triply charged precursor that is stabilized via fission. However, clear evidence for the occurrence of channels involving highly charged sulfur has been found in earlier work on sulfur clusters, where fission following S 1s-excitation was studied [29]. A comparison with the present results indicates that the processes studied in this work are mostly due to fission from doubly charged clusters. This is consistent with related work [6], in which sizable quantities of multiply charged fragments from argon clusters were only found with high intensity, when Xe^{25+} was used as a projectile.

Fragmentation of doubly charged clusters can occur in single- or multiple-step processes, leading to two singly charged fragments, respectively. Different processes can be identified from the geometry of their correlation pattern. This way, it is e.g., possible to differentiate between two-, three-, or four-body fragmentation processes [16,30–32]. Briefly, due to conservation of momentum an ideal two-body dissociation will lead to a line with a slope of −1 in a t_2 vs. t_1 correlation plot, where the length of the pattern is determined by the KER of the fission process.

Three-body fission processes of an initial molecule ABC^{2+} into A, B^+ and C^+ involve the release of neutrals either prior or after the charge separation step. This leads to coincidence patterns with the shape of a parallelogram. The main slope m of the long sides is determined by the mass ratio $m = -m_C/(m_A + m_B)$ or $m = -(m_A + m_B)/m_C$, for the heaviest correlated cation being B^+ or C^+, respectively [30]. Furthermore, the length of the long sides of the parallelogram is determined by the KER of the charge separation step, whereas the length of the short edges mirrors the KER of the neutral moiety.

A four-body fission process in which a doubly charged parent ion $ABCD^{2+}$ breaks up into AB^+ and CD^+, which subsequently decays into $A + B^+$ and $C^+ + D$ will lead to the formation of a coincidence signal of hexagonal shape, if the kinetic momenta of the correlated ions are far smaller than the kinetic momentum of the cations after the charge separation step. The hexagonal pattern will have two horizontal and two vertical edges determined by the kinetic momenta of the neutral emission processes and two oblique edges with a slope $m = -[(m_B/m_A + m_B)\ (m_C + m_D/m_C)]$ or $m = -[(m_C/m_C + m_D)\ (m_A + m_B/m_B)]$, depending on whether B^+ or C^+ is the heavier of the correlated cations. The length L of the inclined edge is determined by [16]:

$$L = \frac{2p_1}{F}\sqrt{\left(\frac{m_C}{m_C + m_D}\right)^2 + \left(\frac{m_B}{m_A + m_B}\right)^2} \quad (2)$$

where p_1 is the momentum of the ions after the charge separation step. The kinetic energy releases of the three steps are determined according to:

$$U_1 = \frac{p_1^2}{2(m_{AB} \cdot m_{CD}/m_{AB} + m_{CD})},$$

$$U_{2-1} = \frac{p_{2-1}^2}{2(m_A \cdot m_B/m_A + m_B)} \quad \text{and}$$

$$U_{2-2} = \frac{p_{2-2}^2}{2(m_C \cdot m_D/m_C + m_D)} \quad (3)$$

where U_{2-1} and U_{2-2} and p_{2-1} and p_{2-2} are the kinetic energy releases and the kinetic momenta corresponding to the loss of neutrals, respectively. U_1 is the KER of the charge separation process.

Assuming that the kinetic energy release is simply the result of electrostatic repulsion, one can determine the charge separation distance (CSD) of the two charges prior to the charge separation sequence (3) using Coulomb's law, $CSD = (1/4\pi\varepsilon_0)\cdot(q_1 \cdot q_2/KER)$, where ε_0 is the dielectric constant of the vacuum and q_1 and q_2 are the repelling charges in units of the elementary charge e.

For the chopper-ion–ion-coincidence experiments we have used ion beams of Xe^{q+}, with $q = 5$, 10, 15, 20, accelerated to 10 kV (for $q = 5$, 10, and 20) and 8 kV (for $q = 15$). In the present paper we will focus on the results obtained from collisions of sulfur clusters with beams of Xe^{5+} and Xe^{20+} and discuss these in comparison to the earlier published data by Teodorescu et al. [16,17].

We have used the procedure presented above for analyzing the experimental sulfur ion coincidence signals, as shown in Figs. 2 and 3, providing plausible fission mechanisms. These correspond to the full lines, which are included in Figs. 2 and 3. Key quantities, which are extracted from the peak shape analysis, are the signal slopes and their widths. These are used to determine kinetic energy releases as well as charge separation distances. The proposed fragmentation mechanisms are discussed in the following (cf. Table 2).

Fig. 2 displays the sulfur cation correlation data as recorded after collisions of free sulfur clusters with a Xe^{5+} ion beam.

Table 1
Relative intensities of mass lines normalized to the intensity of the S_8^+ cation signal, as recorded after ionization with various Xe^{q+} ion beams (see results shown in Fig. 1)

Cation	Xe^{2+}	Xe^{5+}	Xe^{10+}	Xe^{15+}	Xe^{20+}
S_8^+	1	1	1	1	1
S_7^+	0.37	0.04	0.31	0.11	0.03
S_6^+	0.91	0.33	0.65	0.50	0.36
S_5^+	1.02	0.31	0.39	0.42	0.25
S_4^+	3.34	0.65	0.93	0.87	0.75
S_3^+	12.75	0.36	0.83	0.79	0.38
S_2^+	56.80	2.19	2.73	2.16	2.02
S^+	53.24	4.75	3.15	1.12	1.46

The relative intensity of the parent ion is arbitrarily set to unity. The mass signal corresponding to S^+ may contain contributions from residual gas.

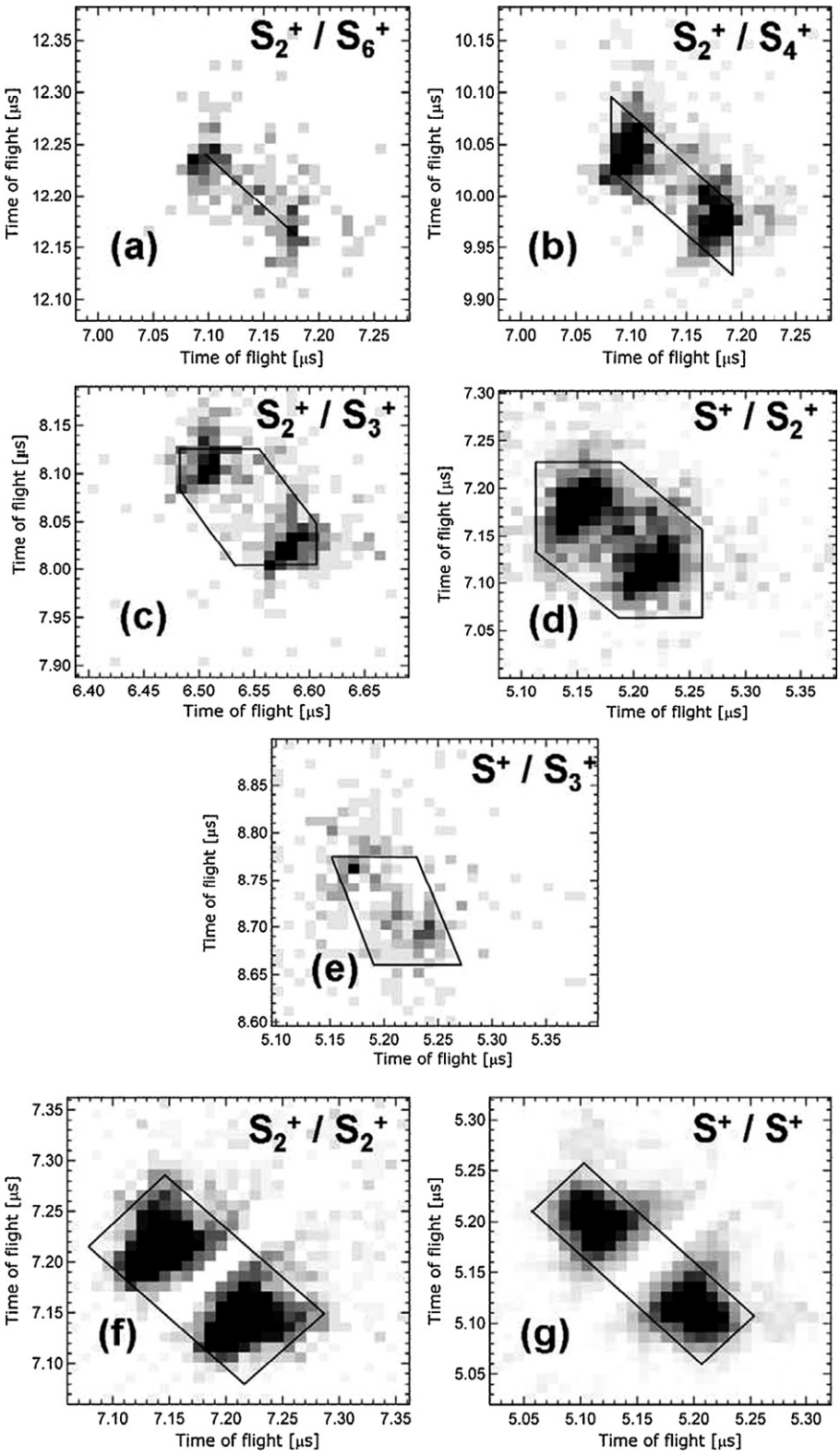

Fig. 2. Chopper-ion–ion-correlation plots of 50 keV Xe^{5+} induced ionization of S_8 (see text for further details).

The ion pairs identified are: S_2^+/S_6^+, S_2^+/S_4^+, S_2^+/S_3^+, S^+/S_2^+, S^+/S_3^+, S_2^+/S_2^+, and S^+/S^+. Fig. 3 shows shapes of the chopper-ion–ion-correlation data of sulfur ion fragments as recorded after ionization with a Xe^{20+} ion beam. The coincidence channels identified are: S_2^+/S_6^+, S_2^+/S_4^+, S_2^+/S_3^+, S^+/S_2^+, S_2^+/S_2^+, and S^+/S^+. Finally, Fig. 4 depicts the puckered ring structure of the S_8 cluster, where the geometry is based on earlier work [32]. The sulfur atoms are numbered in order to ease the understanding of the sites at which the charges are localized prior to charge separation, as deducted from the analysis of the coincidence signals. The major ion pair formation channels are discussed in the following:

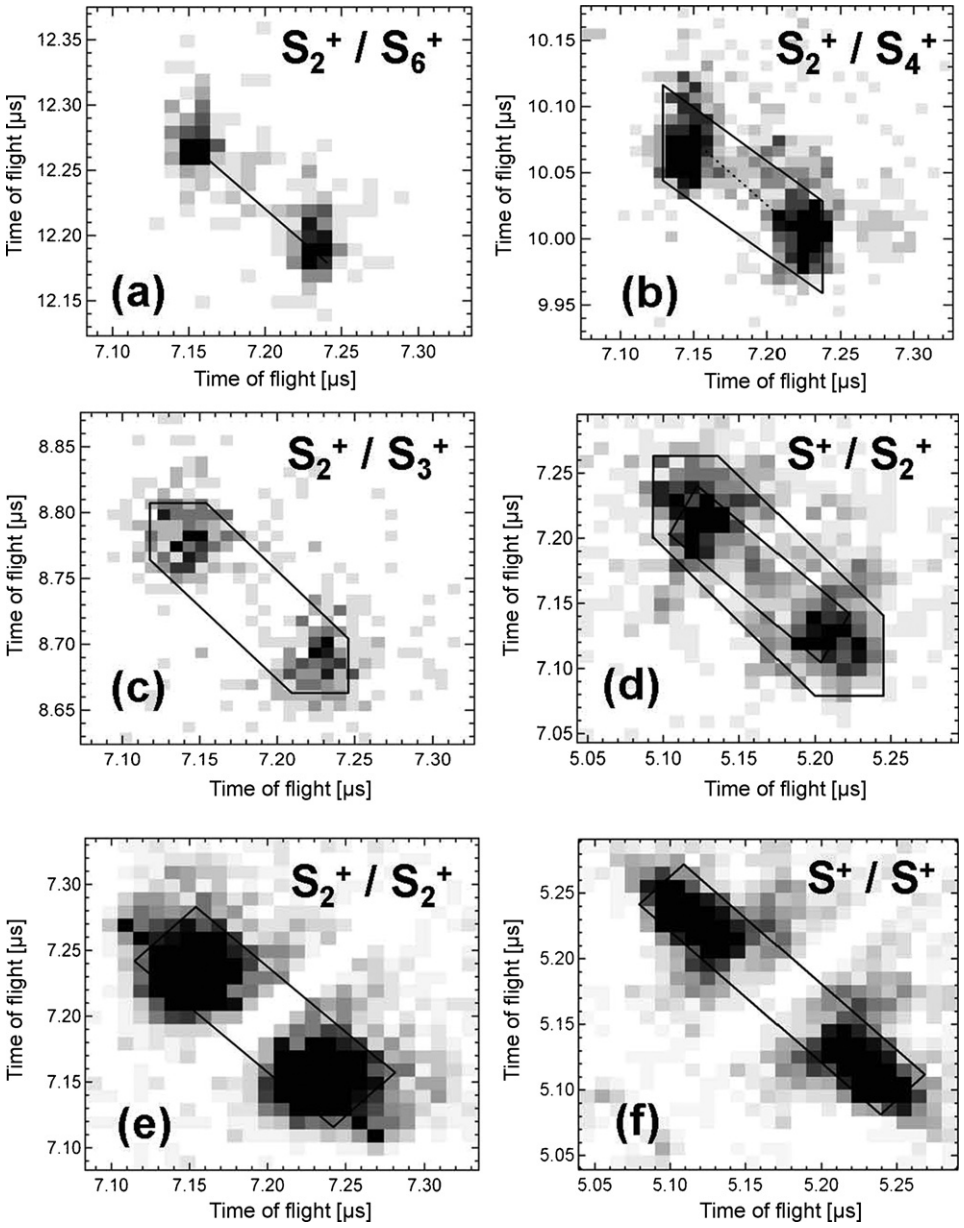

Fig. 3. Chopper-ion–ion-correlation plots of 200 keV Xe^{20+} induced ionization of S_8 (see text for further details).

3.3. (a) The S_2^+/S_6^+ cation pair

Evidence for the occurrence of this weak channel is shown in Figs. 2(a) and 3(a). Earlier work by Teodorescu et al. indicates that the S_2^+/S_6^+ cation pair does not occur as a result of S 2p-excitation [16]. The experimental slope of the correlation plots for Xe^{5+} and Xe^{20+} cases is determined to be in both cases $m = -1.0 \pm 0.1$. This slope is interpreted as a clear indication of a two-body dissociation mechanism which originates from S_8^{2+}.

The kinetic energy release accompanying this fragmentation process is 3.2 ± 0.8 eV which corresponds to a charge separation distance of 4.5 ± 0.9 Å. This result indicates a charge separation where the charges are located at almost opposite sites in the S_8 cluster (e.g., at atoms 1 and 4, cf. Fig. 4) assuming a S–S bond length of 2.055 Å in the stable S_8 D_{3h} isomer [33,34]. We note that this maximum charge separation distance has also been observed for fission of S 2p-excited sulfur clusters [16].

3.4. (b) The S_2^+/S_4^+ cation pair

The coincidence signals of this channel are shown in Figs. 2(b) and 3(b). Ionization by Xe^{20+} yields the S_2^+/S_4^+ coincidence signal long shaped with a main slope $m = -0.9 \pm 0.1$. This is similar

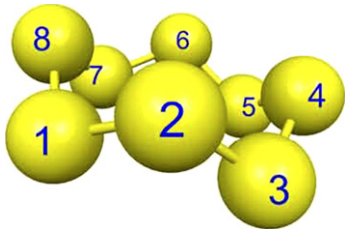

Fig. 4. The puckered ring structure of the S_8 cluster. The sulfur atoms are numbered in order to provide more clarity in the discussion (see text for more details).

Table 2
Peak shape analysis of the ion–ion-coincidence signals shown in Figs. 2 and 3 (see text for further details)

Cation pair	Projectile (relative intensity of fission)	Edge length (ns)	Main edge slope		Proposed mechanism	KER (eV)	CSD (Å)
			Exp.	Calc.			
S_2^+/S_6^+	Xe^{20+} (0.04)	113 ± 14	−1.0 ± 0.1	−1	$S_8^{++} \rightarrow S_6^+ + S_2^+$	3.2 ± 0.8	4.5 ± 0.9
	Xe^{5+} (0.01)	113 ± 14	−1.0 ± 0.1	−1	$S_8^{++} \rightarrow S_6^+ + S_2^+$	3.2 ± 0.8	4.5 ± 0.9
S_2^+/S_4^+	Xe^{20+} (0.13)	144 ± 11	−0.9 ± 0.1	−0.8	$S_7^{++} \rightarrow S_5^+ + S_2^+$	5.2 ± 0.9	2.8 ± 0.4
		73 ± 8			$S_5^+ \rightarrow S_4^+ + S$	2.5 ± 0.6	
		80 ± 14		−1	$S_6^{++} \rightarrow S_4^+ + S_2^+$	3.6 ± 1.4	4.0 ± 1.1
	Xe^{5+}(0.05)	159 ± 13	−1.6 ± 0.1	−1.5	$S_7^{++} \rightarrow S_4^+ + S_3^+$	3.8 ± 0.7	3.8 ± 0.6
		69 ± 10			$S_3^+ \rightarrow S_2^+ + S$	2.7 ± 0.8	
S_2^+/S_3^+	Xe^{20+}(0.05)	138 ± 11	−1.2 ± 0.1	−1.125	$S_7^{++} \rightarrow S_4^+ + S_3^+$	4.2 ± 0.7	3.4 ± 0.5
		40 ± 8			$S_4^+ \rightarrow S_3^+ + S$	0.8 ± 0.4	
		32 ± 8			$S_3^+ \rightarrow S_2^+ + S$	0.6 ± 0.3	
	Xe^{5+}(0.03)	94 ± 14	−1.5 ± 0.2	−1.5	$S_8^{++} \rightarrow S_4^+ + S_4^+$	1.7 ± 0.3	8.5 ± 1.8
		70 ± 10			$S_4^+ \rightarrow S_2^+ + S_2$	1.8 ± 0.6	
		40 ± 10			$S_4^+ \rightarrow S_3^+ + S$	0.8 ± 0.4	
S^+/S_2^+	Xe^{20+}(0.13)	154 ± 11	−1.1 ± 0.1		$S_8^{++} \rightarrow S_5^+ + S_3^+$	4.8 ± 0.7	3.0 ± 0.4
		59 ± 8		−1.125	$S_5^+ \rightarrow S_2^+ + S_3$	1.1 ± 0.3	
		42 ± 8			$S_3^+ \rightarrow S^+ + S_2$	1.0 ± 0.4	
		37 ± 11		2	$S_7^{++} \rightarrow S_3^{++} + S_4$	0.5 ± 0.3	
		130 ± 14		−1	$S_3^{++} \rightarrow S_2^+ + S^+$	9.6 ± 2.2	1.5 ± 0.3
	Xe^{5+}(0.14)	78 ± 14	−1.2 ± 0.2	−1.2	$S_8^{++} \rightarrow S_5^+ + S_3^+$	2.4 ± 0.7	6.0 ± 1.4
		60 ± 10			$S_5^+ \rightarrow S_2^+ + S_3$	1.1 ± 0.4	
		50 ± 10			$S_3^+ \rightarrow S^+ + S_2$	1.4 ± 0.6	
S^+/S_3^+	Xe^{5+}(0.02)	117 ± 13	−3.0 ± 0.3	−3	$S_6^{++} \rightarrow S_3^+ + S_3^+$	2.4 ± 0.5	6.0 ± 1.0
		80 ± 10			$S_3^+ \rightarrow S^+ + S_2$	3.6 ± 1.0	
S_2^+/S_2^+	Xe^{20+}(0.36)	56 ± 14	1.0 ± 0.2	1	$S_8^{++} \rightarrow S_4^{++} + S_4$	1.2 ± 0.3	
		183 ± 14	−1.0 ± 0.1	−1	$S_4^{++} \rightarrow S_2^+ + S_2^+$	6.3 ± 1.0	2.3 ± 0.3
	Xe^{5+}(0.24)	67 ± 14	1.0 ± 0.2	1	$S_8^{++} \rightarrow S_4^{++} + S_4$	1.7 ± 0.5	
		134 ± 14	−1.0 ± 0.1	−1	$S_4^{++} \rightarrow S_2^+ + S_2^+$	3.4 ± 0.8	4.2 ± 0.8
S^+/S^+	Xe^{20+}(0.29)	42 ± 14	1.0 ± 0.2	1	$S_8^{++} \rightarrow S_2^{++} + S_6$	0.9 ± 0.7	
		212 ± 14	−1.0 ± 0.1	−1	$S_2^{++} \rightarrow S^+ + S^+$	8.5 ± 1.2	1.7 ± 0.2
	Xe^{5+}(0.51)	56 ± 14	1.0 ± 0.2	1	$S_8^{++} \rightarrow S_2^{++} + S_6$	1.6 ± 0.9	
		183 ± 14	−1.0 ± 0.1	−1	$S_2^{++} \rightarrow S^+ + S^+$	6.3 ± 1.0	2.3 ± 0.3

to previous PEPIPICO results [16]. An experimental slope smaller than −1 indicates a secondary decay process involving the heavier cation [30]. The parallelogram in Fig. 3(b) may thus correspond to the fission of S_7^{++}, into S_5^+ and S_2^+. This would be followed by a dissociation of the intermediate S_5^+ ion into $S_4^+ + S$. However, the secondary decay scenario does not completely describe the experimental data since this process would lead to a slope of −0.8, as observed in previous inner-shell fragmentation work [16]. The S_2^+/S_4^+ cation pair could also be due to two-body dissociation of S_6^{++}. This process is represented in Fig. 3(b) by the dashed line with a slope $m = -1$. No other plausible fragmentation channel originating from S_8 would yield the experimentally observed slope. Therefore it is a straightforward conclusion that the S_2^+/S_4^+ ion pair is the result of two competing processes. This yields a superposition of the pathways described above. Based on the size distribution of neutrals in the cluster beam, it can be assumed that both S_7^{++} and S_6^{++} are formed from S_8^{++} by the loss of the neutrals S and S_2 or 2 S prior to fission. The kinetic energy release which accompanies the two paths are 5.2 ± 0.9 eV for the three-body process and 3.6 ± 1.4 eV for the two-body mechanism, which correspond to charge separation distances of 2.8 ± 0.4 Å and 4.0 ± 1.1 Å, respectively. These charge separation distances indicate that the charges are either located at adjacent sites (sites 1 and 2 in Fig. 4) or second neighboring (e.g., at sites 1 and 3 in Fig. 4), respectively. Finally, the loss of the neutral from the intermediate S_5^+ ion is accompanied by a kinetic energy release of 2.5 ± 0.6 eV.

If Xe^{5+} is used for ionizing S_8, the main slope of the S_2^+/S_4^+ pattern is considerably larger, i.e., $m = -1.6 \pm 0.1$. This suggests that the process leading to the correlation plot shown in Fig. 2(b) is a secondary decay of S_7^{++} involving the lighter cation. In a first step, the parent dication breaks up into S_4^+ and S_3^+. In a subsequent step the S_3^+ cation loses a neutral atom. This charge separation process is accompanied by the release of 3.8 ± 0.7 eV, which corresponds to a charge separation distance prior to the fission of 3.8 ± 0.6 Å. This charge separation distance suggests a localization of the charges at second neighboring sites in the cluster (e.g., at atoms 1 and 3 in Fig. 4) before the charge separation step. The loss of the neutral moiety is accompanied by a smaller kinetic energy release, corresponding to 2.7 ± 0.8 eV.

3.5. (c) The S_2^+/S_3^+ cation pair

The coincidence signals of the S_2^+/S_3^+ ion pair are shown in Figs. 2(c) and 3(c). The experimental main slope obtained from ionization by Xe^{20+} is determined to be $m = -1.2 \pm 0.1$. A similar slope has been observed in earlier inner-shell excitation induced fragmentation [16]. The slope indicates a fragmentation process involving at least three fragments. A slope larger than −1 indicates that the secondary loss of a neutral originates from the lighter cation, as mentioned above [30,31]. However, there is no three-body process that can explain the fragmentation process from S_8 leading to the experimental slope, since the minimum slope for such secondary decay would be −1.5, corresponding to the release of a neutral atom. The loss of heavier neutrals or several atoms would lead to even higher slopes. Thus, it appears to be reasonable that the process leading to the appearance of this correlated cation pair

involves the release of neutrals from both cations subsequent to charge separation. This corresponds to a secondary decay in competition originating from S_7^{++}, similar to previous observations in photon-induced fragmentation work [16]. Such a fission process leads to a hexagonal correlation pattern, as depicted in Figs. 2(c) and 3(c).

The kinetic energy release from the charge separation process is calculated to be 4.2 ± 0.7 eV, which corresponds to a charge separation distance in the intermediate dication S_7^{++} of 3.4 ± 0.5 Å. This assignment considers the low mixing ratio of S_7 in the neutral cluster beam [22,23] as a possible neutral parent of S_7^{++}. The loss of neutral moieties after fission is rather accompanied by a small kinetic energy release of 0.8 ± 0.4 eV for the loss of S from the decay of S_4^+ and 0.6 ± 0.3 eV for the loss of S from the S_3^+, respectively.

The experimental main slope for the S_2^+/S_3^+ correlation channel is $m = -1.5 \pm 0.2$, in the case of the ionization by a Xe^{5+} ion beam. This is different from previous work [16] as well as the results from Xe^{20+}-induced fragmentation. Similar to the case of ionization by Xe^{20+} it is concluded that the correlated cations occur as a result of a loss of the neutral S_2 (or 2 S) and S from S_4^+. Note that we cannot distinguish whether a dimer or two atoms are released. It is clear from the results, however, that the loss of the neutrals happens after the charge separation in S_8^{++}. The KER of the break up of S_8^{++} is determined to be 1.7 ± 0.3 eV, corresponding to a CSD of 8.5 ± 1.8 Å prior to fission. Such a charge separation distance is a clear indication that both charges are localized at opposite sites in the doubly charged parent ion (e.g., atoms 1 and 5 in Fig. 4). As a result, the kinetic energy released is comparable to the other fission processes, namely 1.8 ± 0.6 eV for the release of S_2 (or 2 S) and 0.8 ± 0.4 eV for the loss of S.

3.6. (d) The S^+/S_2^+ cation pair

The coincidence signals of the S^+/S_2^+ ion pair are shown in Figs. 2(d) and 3(d). The experimental main slope obtained from the coincidence signal by ionization with Xe^{20+} is $m = -1.1 \pm 0.1$. This is interpreted as evidence for two competing processes. The first one is a secondary decay in competition originating from S_8^{++}, which would lead to a slope of $m = -1.125$, as depicted in Fig. 3(d) by a hexagon (process 1). The second process is a deferred charge separation process starting from S_7^{++} which would result in a main slope of $m = -1$ and a secondary slope which equals 2. It is given by the mass ratio of the fragments emerging from the second step of the deferred charge separation process [35,36]. This process is represented in Fig. 3(d) by a rectangle (process 2). The proposed mechanisms for these fragmentation paths involve the loss of S_3 and S_2 or S_5 (or the corresponding number of atoms bound in smaller molecular fragments or atoms), respectively. Evidence for such a mechanism has not been found in earlier PEPIPICO work, where the main slope of this fairly intense cation pair is -1 [16]. Evidently, this process proceeds in a different way in the case of highly charged ions.

The kinetic energy released in the charge separation steps of the two processes are determined to be 4.8 ± 0.7 eV (process 1) and 9.6 ± 2.2 eV (process 2), corresponding to charge separation distances of 3.0 ± 0.4 Å and 1.5 ± 0.3 Å, respectively. The last two steps of process 1 are accompanied by small kinetic energy releases of 1.1 ± 0.3 and 1.0 ± 0.4 eV, respectively. For the first stage of process 2 a kinetic energy release of 0.5 ± 0.3 eV is determined from the present results.

A fragmentation path similar to process 1 is considered to be also responsible for the occurrence of the S^+/S_2^+ coincidence channel after collisions with Xe^{5+}, where the experimental main slope is determined to be $m = -1.2 \pm 0.2$. The determined KER is 2.4 ± 0.7 eV, corresponding to a charge separation distance of 6.0 ± 1.4 Å. The CSD indicates that prior to the charge separation step, the charges are located at opposite sites in the parent cluster (e.g., atoms 1 and 5 in Fig. 4). A fairly low kinetic energy release of 1.1 ± 0.4 eV is determined for the loss of neutral S_3 and of 1.4 ± 0.6 eV for the loss of neutral S_2.

3.7. (e) The S^+/S_3^+ cation pair

The correlation data for the S^+/S_3^+ ion pair are shown in Fig. 2(e). Note that the S^+/S_3^+ coincidence channel only occurs after ionization by Xe^{5+} with weak intensity. There is also no evidence for this channel in earlier PEPIPICO work [16]. The experimental main slope of this pattern is determined to be $m = -3.0 \pm 0.3$. A plausible mechanism explaining the experimental slope involves a symmetric breakup of S_6^{++}, which is followed by a release of a dimer (or two atoms) from one of the singly charged trimers. Considering the composition of the neutral sulfur vapor [22,23], it is considered that the intermediate dication S_6^{++} originates from S_8^{++} by a release of S_2. The kinetic energy release that accompanies the charge separation process is 2.4 ± 0.5 eV, which corresponds to a charge separation distance prior to the dissociation of 6.0 ± 1.0 Å. This implies that the charges are located at opposite sites in the parent cluster. The release of the neutral S_2 takes place with a kinetic energy release of 3.6 ± 1.0 eV.

3.8. (f) The S_2^+/S_2^+ cation pair

The correlation data for the S_2^+/S_2^+ cation pair are shown in Figs. 2(f) and 3(e). This channel is observed to be more intense than the asymmetric fission channels discussed above. The experimentally determined main slope for this ion pair after ionization with the Xe^{20+} ion beam is $m = -1.0 \pm 0.1$, suggesting a two-body process. This is in agreement with earlier PEPIPICO work [16]. Considering the composition of the sulfur vapor at the temperature used throughout the experiments, we can consider the doubly charged tetramer S_4^{++} as originating from S_8^{++} via a loss of S_4 (or smaller units of the same mass) This is consistent with the finding that the secondary slope of the correlation plot, as derived from Fig. 3(e) by a rectangle, is $\beta = 1.0 \pm 0.2$.

The kinetic energy released in the charge separation process is 6.3 ± 1.0 eV, which corresponds to a charge separation distance of 2.3 ± 0.3 Å prior to the dissociation (e.g., sites 1 and 2 in Fig. 4). The loss of the S_4 aggregate in the first stage of the fission is accompanied by a kinetic energy release of 1.2 ± 0.3 eV. These results are in agreement with earlier PEPIPICO work [16], indicating that the fission mechanisms are identical.

In a similar way, it is evident for ionization by Xe^{5+}, that the process leading to the experimental observed main slopes of $m = -1.0 \pm 0.1$ and $\beta = 1.0 \pm 0.2$ is also a deferred charge separation, with the intermediate formation of S_4^{++}. The KER corresponding to the two steps are is 1.7 ± 0.5 eV and 3.4 ± 0.8 eV, respectively. The CSD in the doubly charged cation is inferred to be 4.2 ± 0.8 Å, which indicates that the charges are located at 'almost opposite' sites in the cluster (e.g., atoms 1 and 4 in Fig. 4). In addition, these results appear to be still in agreement with earlier photoexcitation work [16]. In this earlier work, the charge separation distance was rather interpreted to be related to an intermediate S_4^{2+}, which consists of a van der Waals dimer of two S_2 moieties. Evidence for this assumption came from earlier theoretical work, which assigned the structure of this species [33,34,37]. However, the present results yield a lower KER, so that the CSD is more plausibly related to S_8^{2+} than to S_4^{2+}.

3.9. (g) The S^+/S^+ cation pair

The coincidence signals of the S^+/S^+ ion pair are shown in Figs. 2(g) and 3(f). Similar to the S_2^+/S_2^+-channel, this channel is also more intense than the asymmetric fission channels. The S^+/S^+ coincidence patterns have a main slope of $m = -1.0 \pm 0.1$. Considering that S_8 is the major component in the gas phase at the experimental evaporation temperature [22,23], it is considered to be quite unlikely that this cation pair is due to a two-body dissociation of the possible parent S_2^{++}, but instead originates from S_2^{++} formed via a decay of S_8^{++}. This conclusion is also supported by the secondary slope of the correlation plots of $\beta = 1.0 \pm 0.2$.

The kinetic energy released in the charge separation process is 8.5 ± 1.2 eV for the Xe^{20+} case and 6.3 ± 1.0 eV for the Xe^{5+} case, corresponding to a charge separation distance of 1.7 ± 0.2 Å and 2.3 ± 0.3 Å, respectively. The charge separation distances imply a localization of the charges in the doubly charged dimers at neighboring sites. The loss of S_6 (or the corresponding number of smaller molecular or atomic units) in the first stage before fission is accompanied by a KER of 0.9 ± 0.7 eV and 1.6 ± 0.9 eV, respectively. These results on the S^+/S^+ ion pair are similar in magnitude compared to earlier work on S 2p-excitation [16], indicating that this process occurs quite independent of the primary ionization. We note that in earlier work [16] a slope of −4 was observed, which is not observed upon impact by highly charged ions. This was assigned in terms of a secondary decay of S_5^{++}, which is likely formed from S_8^{++}.

4. Conclusions

We present experimental data that shed light onto the fission processes of S_8 induced by highly charged ions. These are to a large extent, remarkably similar in their dynamics to earlier photon-induced PEPIPICO work [16]. This result is unexpected, since the underlying multiple ionization mechanisms are entirely different. The photon-induced inner-shell excitation, communicated in Ref. [16], starts with a well-defined site within the cluster. Auger relaxation leads to holes in the valence shell, which are followed by fission leading eventually to the formation of singly charged products. In the S 2p-regime double ionization is the dominant process. In contrast, ionization by HCI leads to the loss of electrons from the outer valence shell levels, which are expected to be delocalized over the entire molecular system. It is expected that the loss of electrons depends on the charge of the projectile: For low projectile charge state, capture takes place at short distances and is accompanied by electronic excitation whereas for high projectile charges states, capture occurs at large distances and leaves the target further unaffected. In any case, as a result a S_8 moiety can break up into several charged fragments. The present work, however, selects only those processes, which lead to correlated pairs of fragments, so that similar product channels as in PEPIPICO experiments are accessed. As a result, it is not entirely surprising that there are not too many differences between both complementary approaches.

One important aspect to point out is that in highly charged ion induced ionization we have observed evidence for direct two-body dissociation of S_8^{++} into $S_2^+ + S_6^+$. This channel is not observed in earlier work on inner-shell excited sulfur clusters [16]. This coincidence channel occurs only when the two charges are localized at almost opposite sites in the doubly charged parent ion, which appears to be a favorable situation upon ionization via HCI.

A comparison of the present results indicates that the initial charge localization in the doubly charged parent cluster can be related to the selective charge separation processes into singly charged fragments. Specifically, we have observed for the Xe^{5+} ion beam case, that the localization of the charges at opposite sites leads to the occurrence of S_3^+ in coincidence with other charged moieties. The second ionic species, i.e., S^+ or S_2^+, depends on whether the parent ion has released a neutral prior to charge separation. The localization of the charges in the parent dication at second neighboring positions leads to the appearance of the S_2^+/S_4^+ coincidence channel, with the intermediate formation of the S_7^{2+} aggregate.

In the case of ionization by Xe^{20+}, we have observed that when the two charges are located at second neighboring sites before fission, the coincidence channels are S_2^+/S_3^+ and S^+/S_2^+, irrespective of the parent dication. When the charges are localized at second neighboring sites in the parent dication and it is releasing a neutral moiety prior to charge separation, the fragmentation process will lead to the appearance of the S_2^+/S_4^+ cation pair. It has also been observed that when the charges in the parent ion are localized at adjacent sites, the doubly charged ion can undergo fission via a two-body dissociation mechanism leading to the S_2^+/S_4^+ cation pair.

The symmetric S^+/S^+ coincidence channel only occurs when the two charges are located in the parent ion at neighboring positions prior to fission, in a similar manner to fission which is followed by S 2p-excitation [16]. The occurrence of this channel is irrespective of the charge of the ion beam projectile.

Acknowledgments

Financial support from the German Ministry for Education and Research (BMBF project number 05KS4WWD/0) is gratefully acknowledged. This experiment has been performed at the ZERNIKE-LEIF, part of the distributed LEIF infrastructure. The support received by the European Project ITS LEIF (RII3/026015) is gratefully acknowledged.

References

[1] H. Haberland (Ed.), 'Clusters of Atoms and Molecules', vols. I and II, Springer Ser. Chem. Phys., vols. 52 and 56, Springer, Berlin (1994, 1995).
[2] T. Kondow, F. Mafuné (Eds.), Progress in Experimental and Theoretical Studies of Clusters, World Scientific, Singapore, 2003.
[3] E. Rühl, Int. J. Mass Spectrom. 229 (2003) 117.
[4] E. Rühl, C. Schmale, H.-W. Jochims, E. Biller, M. Simon, H. Baumgärtel, J. Chem. Phys. 95 (1991) 6544.
[5] E. Rühl, C. Heinzel, H. Baumgärtel, M. Lavollée, P. Morin, Z. Physik D. 31 (1994) 245.
[6] W. Tappe, R. Flesch, E. Rühl, R. Hoekstra, T. Schlathölter, Phys. Rev. Lett. 88 (2002) 143401.
[7] A. Ding, J. Hesslich, Chem. Phys. Lett. 94 (1983) 54;
U. Näher, S. Frank, N. Malinowski, U. Zimmermann, T.P. Martin, Z. Physik D. 31 (1994) 191.
[8] T. Jahnke, A. Czasch, M.S. Schöffler, S. Schössler, A. Knapp, M. Käsz, J. Titze, C. Wimmer, K. Kreidi, R.E. Grisenti, A. Staudte, O. Jagutzki, U. Hergenhahn, H. Schmidt-Böcking, R. Dörner, Phys. Rev. Lett. 93 (2004) 163401.
[9] H. Wabnitz, L. Bittner, A.R.B. de Castro, R. Döhrmann, P. Gürtler, T. Laarmann, W. Laasch, J. Schulz, A. Swiderski, K. von Haeften, T. Möller, B. Faatz, A. Fateev, J. Feldhaus, C. Gerth, U. Hahn, E. Saldin, E. Schneidmiller, K. Sytchev, K. Tiedtke, R. Treusch, M. Yurkov, Nature 420 (2002) 482.
[10] O. Hadjar, R. Hoekstra, R. Morgenstern, T. Schlathölter, Phys. Rev. A 63 (2001) 033201.
[11] Y. Levy, I. Last, J. Jortner, Proc. Natl. Acad. Sci. U.S.A. 99 (2002) 9107.
[12] Y. Levy, I. Last, J. Jortner, Mol. Phys. 104 (2006) 1227.
[13] K. Nagaya, M. Yao, T. Hayakawa, Y. Ohmasa, Y. Kajihara, M. Ishii, Y. Katayama, Phys. Rev. Lett. 89 (2002) 243401.
[14] K. Nagaya, A. Oohata, I. Yamamoto, M. Yao, J. Non-Cryst. Solids 312–314 (2002) 337.
[15] K. Nagaya, J. Phys. Soc. Jpn. 72 (2003) 501.
[16] C.M. Teodorescu, D. Gravel, E. Rühl, J. Chem. Phys. 109 (1998) 9280.
[17] C.-M. Teodorescu, D. Gravel, J. Choi, D. Pugmire, P.A. Dowben, N. Fominykh, A.A. Pavlychev, E. Rühl, J. Electron Spectrosc. Relat. Phenom. 101–103 (1999) 193.
[18] E. Rühl, R. Flesch, W. Tappe, D. Novikov, N. Kosugi, J. Chem. Phys. 116 (2002) 3316.

[19] J. Daligault, F. Chandezon, C. Guet, B.A. Huber, S. Tomita, Phys. Rev. A 66 (2002) 033205;
S. Martin, L. Chen, J. Bernard, M.C. Buchet-Poulizac, B. Wei, R. Brédy, Phys. Rev. A 73 (2006) 013204.
[20] T. Schlathölter, F. Alvarado, R. Hoekstra, Nucl. Instrum. Meth. B 233 (2005) 62;
K. Tabayashi, S. Tada, J. Aoyama, K. Saito, H. Yoshida, S. Wada, A. Hiraya, K. Tanaka, J. Electron. Spectrosc. Relat. Phenom. 144–147 (2005) 179;
C. Harada, S. Tada, K. Yamamoto, Y. Senba, H. Yoshida, A. Hiraya, S. Wada, K. Tanaka, K. Tabayashi, Rad. Phys. Chem. 75 (2006) 2085.
[21] T. Schlathölter, R. Hoekstra, R. Morgenstern, J. Phys. B: At. Mol. Opt. Phys. 31 (1998) 1321.
[22] J. Berkowitz, J.R. Marquart, J. Chem. Phys. 39 (1963) 275.
[23] J.R. Marquart, J. Berkowitz, J. Chem. Phys. 39 (1963) 283.
[24] J. Berkowitz, W.A. Chupka, J. Chem. Phys. 40 (1964) 287.
[25] J. Berkowitz, C. Lifshitz, J. Chem. Phys. 48 (1968) 4346.
[26] W.C. Wiley, I.H. McLaren, Rev. Sci. Instr. 26 (1955) 1150.
[27] B. Siegmann, U. Werner, H.O. Lutz, R. Mann, J. Phys. B: At. Mol. Opt. Phys. 34 (2001) L587.
[28] F. Alvarado, R. Hoekstra, T. Schlathölter, J. Phys. B: At. Mol. Opt. Phys 38 (2005) 4085.
[29] M. Kuhlmann, Diploma Thesis, University of Osnabrück, Onabrück, 1999.
[30] J.H.D. Eland, Mol. Phys. 61 (1987) 725.
[31] M. Simon, T. Lebrun, R. Martins, G.G.B. de Souza, I. Nenner, M. Lavollée, P. Morin, J. Phys. Chem. 97 (1993) 5228.
[32] E. Rühl, S.D. Price, S. Leach, J.H.D. Eland, Int. J. Mass Spectrom. Ion Proc. 97 (1990) 175.
[33] K. Raghavachari, C. McMichael Rohlfing, J.S. Binkley, J. Chem. Phys. 93 (1990) 5862.
[34] S.J. Rettig, J. Trotter, Acta Cryst. C 43 (1987) 2260.
[35] J.H.D. Eland, Laser Chem. 11 (1991) 259.
[36] M. Lavollée, H. Bergeron, J. Phys. B: At. Mol. Opt. Phys. 25 (1992) 3101.
[37] B.C. Pan, C.K. Duan, S.D. Xia, C.Y. Xiao, Phys. Rev. B 50 (1994) 17556.